ADVANCED MATERIALS INTERFACES
www.advmatinterfaces.de

Interfacial Engineering of Van der Waals Coupled 2D Layered Materials

*Hao Hong, Can Liu, Ting Cao, Chenhao Jin, Shaoxin Wang, Feng Wang, and Kaihui Liu**

Engineering the properties of materials is of central importance in modern science and technology. In conventional bulk materials, the property changes are realized mainly through modifying the chemical bonds and crystalline structures, or introducing dopant atoms. Recent studies in van der Waals coupled 2D layered materials have demonstrated a different way of materials engineering through modifying interlayer interactions at the material interfaces, because the interlayer interactions in these materials can be easily controlled by changing interlayer stacking configurations and/or applying external fields. In this review, recent progresses in exploring the effects of van der Waals interlayer interactions on graphene, including the discovery of van Hove singularities, Fermi velocity renormalization, and Hofstadter's butterfly pattern, are discussed. Interlayer interactions at other 2D layered material interfaces, such as transition metal dichalcogenides and black phosphorus, are also discussed. Finally, the prospects of using the van der Waals coupled 2D layered materials for next-generation electronics and optoelectronics are presented.

1. Introduction

Recent studies on van der Waals coupled 2D layered materials have unveiled a wide range of novel phenomena distinctly different from their bulk counterparts.[1–6] Engineering the properties of these materials, in particular through the interlayer interactions, has opened up a new regime of materials engineering. In sharp contrast to conventional bulk materials, the interlayer interactions in van der Waals coupled materials can be controlled mainly by two approaches, that is, designing interlayer stacking configurations[7–9] and/or applying external fields.[10,11] The former approach relies on the relatively weak van der Waals interaction between neighboring layers. Compared with the interfaces of bulk semiconductors, where strong covalent or ionic bonds between heteroatoms lead to a well-aligned interface, van der Waals coupled materials can have various stacking configurations with different twist angle between neighboring layers. These twist structures can either be realized by direct growth methods or controlled by transfer methods. The latter approach for engineering interlayer interactions relies on the convenience to electrically gate ultrathin van der Waals coupled layers. When a gate voltage is applied along the out-of-plane direction, the displacement field between the layers can be as large as 0.3 V Å^{-1}. For van der Waals coupled materials, both approaches are effective in tuning their electronic, mechanical, optical properties, etc. The band structures can be easily modified, since the hybridization of the electronic states from adjacent layers significantly depends on both the stacking configuration and the out-of-plane electric field.

Recent experiments have demonstrated the unusual effects of the interlayer van der Waals coupling in a number of 2D materials. For example, in bilayer graphene, by changing the relative twist angle between the two layers, van Hove singularities (vHs) emerge in its band structure.[7] Furthermore, the energy of the vHs is controllable by the twist angle. More recently, in bilayers transition metal dichalcogenide (TMDCs), the circularly polarized photoluminescence (PL) can be continuously tuned via an electrical field applied perpendicular to the 2D film.[11] Indeed, van der Waals coupling of atomically thin 2D layers is of significant promise in the contemporary material engineering. It provides us with a new path to realize high-performance electronic, photovoltaic, photonics, and optoelectronic devices, for example, field-effect transistor and light-emitting diodes based on different 2D layers stacking are designed to realize flexible and transparent electronics;[12–14] MoS_2/WS_2 heterostructure can be operated as a p-n diode;[15–17] TMDCs/graphene was addressed as high quantum efficiency light-harvesting devices.[18–20] The research in 2D materials is

H. Hong, C. Liu, S. X. Wang, Prof. K. H. Liu
State Key Laboratory for Mesoscopic Physics
Collaborative Innovation Center of Quantum Matter
School of Physics
Peking University
Beijing 100871, China
E-mail: khliu@pku.edu.cn
C. Liu, Prof. K. H. Liu
Academy for Advanced Interdisciplinary Studies
Peking University
Beijing 100871, China
T. Cao, C. H. Jin, Prof. F. Wang
Department of Physics
University of California at Berkeley
Berkeley, CA 94720, USA
T. Cao, Prof. F. Wang
Materials Sciences Division
Lawrence Berkeley National Laboratory
Berkeley, CA 94720, USA
Prof. K. H. Liu
Centre for Nanochemistry
College of Chemistry and Molecular Engineering
Peking University
Beijing 100871, China

DOI: 10.1002/admi.201601054

also rapidly developing due to the expanding family of 2D material species, ranging from metallic single-layer $NbSe_2$, semimetallic graphene, to semiconducting single-layer TMDCs and insulating hexagonal boron nitride(h-BN). As such, the degree of freedom in choosing the components in constructing the van der Waals coupled heterostructures leads to a variety of material systems. This diversity makes the interfacial engineering in 2D more appealing than that in 3D or 1D system, as interfacial engineering in 1D has so far only been experimentally achieved in double-wall carbon nanotubes.[21,22]

Here, we review how the properties of graphene are modified via van der Waals interfacial engineering, including interlayer electronic states hybridization and periodical potential modification. Besides, the cases of other 2D layered material are discussed, such as phosphorene, TMDCs, and TMDCs heterostructures. Finally, we present the prospects of using the van der Waals coupled 2D materials for next-generation electronics and optoelectronics.

2. Van der Waals Coupling in Graphene

2.1. Electronic Properties of Monolayer Graphene and AB-Stacking Bilayer Graphene

Graphene, a single layer of sp^2-hybridized carbon atoms bonded into a honeycomb structure, is the first atomically thin 2D layer to be investigated extensively.[23–26] The unique structural configuration of graphene gives rise to exotic properties, such as excellent mechanical strength,[27–29] ultrahigh thermal conductivity,[30–33] broadband light transmittance,[34–37] and so on. Due to these remarkable material properties, graphene has attracted intense research interests in the past decade, and is likely to remain one of the leading research topics in the next decade. For potential applications of graphene, tailoring its electronic properties is of great significance.

The honeycomb structure of graphene is composed of two interpenetrating triangular Bravais lattices (**Figure 1**a). Three of four carbon atomic valence electrons form σ bands with sp^2 hybridization, while the left p_z orbital develops into π and π^* bands close to the Fermi energy. The π band energy dispersion is in the form of a conical shape around the zero energy K and K′ points (the Dirac points), which are responsible for the novel properties of graphene (Figure 1b).

With one more layer added, bilayer graphene exhibits much different properties. The electronic states in both layers are in the same energy range, the interlayer electronic coupling mainly manifests as direct hybridization between interlayer electronics states. Electronic states from one layer can directly couple to the states from the other layer, which will be the strongest in the degenerate coupling case, giving new features such as vHs.

Configurations of AA-stacking/twisted/AB-stacking bilayer graphene are shown in Figure 1d. In AA (AB) stacking, the A→B bond directions are the same (opposite) for the two layers, while in twist stacking, the A→B bond directions have a relative angle ($0 < \theta < 180°$). They can be directly obtained by chemical vapor deposition (CVD) growth,[38–43] mechanical exfoliation of graphite,[44–46] or precise transfer techniques.[47,48]

Hao Hong received his B.S. degree from Shandong University and then he joined the Ultrafast Nano-optics group of Prof. Kaihui Liu in 2014. His research interests are characterizing light–matter interactions and physical properties of low-dimensional nanomaterials and material interfaces through optical method.

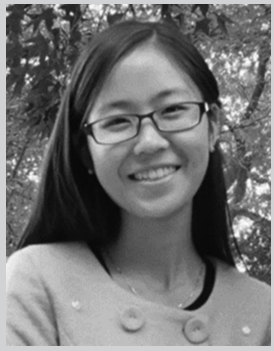

Can Liu received her B.S. degree from Northwestern Polytechnical University in 2014. Now she is a Ph.D. candidate under the supervision of Prof. Kaihui Liu in School of Physics, Peking University, Beijing, China. Her research interests mainly focus on the preparation and investigation of optical properties of low-dimensional nanomaterials, including carbon nanotubes and graphene.

Kaihui Liu received his Ph.D. from Institute of Physics, Chinese Academy of Sciences in 2009. After a postdoctoral fellowship at UC Berkeley, USA, he joined Peking University as the National Thousand Youth Talents Plan Professor of China (2014). Prof. Kaihui Liu's main research interests are the novel physical phenomena and controllable growth in nanomaterials, especially in 1D carbon nanotubes and 2D graphene. He developed an advanced single nano-object level in situ Nano-optics + TEM technique, and in situ Nano-optics + CVD technique to study structure-dependent physics and growth mechanism at nanoscale.

Among them, the AB-stacking structure (also known as the Bernal stacking in graphene) is the most energetically favorable configuration. The modification of the band structure in the AB-stacking bilayer graphene comes from the electron hopping between the two freestanding monolayers. Because of the interlayer electron hopping, the linearly dispersive and twofold degenerate π and π^* bands split into four nearly parabolic bands, π_1, π_1^*, π_2, and π_2^* (Figure 1c). Within the valleys, the two conduction bands (π_1^* and π_2^*) are nearly parallel to each

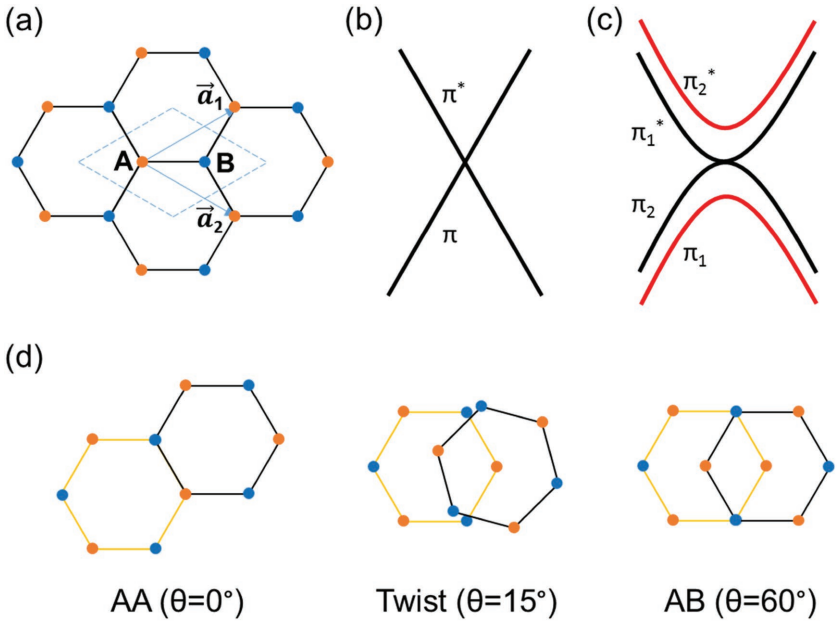

Figure 1. a) Lattice structure of graphene, $\mathbf{a_1}$ and $\mathbf{a_2}$ are the lattice unit vectors. Orange (blue) ball stands for A (B) atom of graphene. Low-energy band structure of b) monolayer and c) AB-stacking bilayer graphene. d) Configurations of AA-stacking/twisted/AB-stacking bilayer graphene. Gold and black hexagons belong to different layers.

other, so are the two valence bands (π_1 and π_2). In the absence of an external electric field, the top valence band and bottom conduction band touch each other at the K and K′ points of the Brillouin zone. When an external electric field is applied along the out-of-plane direction, the two graphene layers are no longer protected by the inversion symmetry. As a result, an energy gap will be opened in the valleys.[10,44,45,49]

2.2. Van Hove Singularities in Twisted Bilayer Graphene

Low-energy band structure of bilayer graphene is extremely sensitive to the stacking order. In twisted bilayer graphene, the twist angle between the two overlaid layers would introduce a moiré pattern with a much larger period than the graphene lattice (**Figure 2**a). The Brillouin zones of the two layers are also rotated by the same angle relative to each other, as shown in Figure 2b. Therefore, the two Dirac cones separated by ΔK touch each other, with the lowest energy touching points forming two saddle points with positive and negative energies, respectively. The saddle points in the energy momentum landscape contribute to the vHs in the density of states (DOS) spectra, shown as the two pronounced peaks in Figure 2b.[50,51] In the situations where the twist angle is very small ($\theta \leq 1°$), the DOS peaks are very close to the Dirac points.[52,53] As a result, the electron bands between the two Dirac points of the top and bottom layers are only weakly dispersive.

Li et al.[7] first observed vHs in twisted bilayer graphene by means of scanning tunneling spectroscopy (STS) and Landau level spectroscopy. After that, Yan et al.[54] and Brihuega et al.[55] showed these singularities are angle dependent and can be explained by tight-binding calculations. Raman spectroscopy was also used to study the vHs and provides a new view on investigating the electronic band structure of twisted bilayer graphene.[56,57] The moiré period revealed by STM varies with the twist angle of bilayer graphene (Figure 2c). By detecting the tunneling differential conductance $\mathrm{d}I/\mathrm{d}V$, STS is used to provide information about the local DOS as a function of energy. The two sharp peaks with an energy separation ΔE_{vHs} in DOS curve correspond to the rotation-induced vHs (Figure 2d,e). The larger the twist angle is, the more separation the two Dirac cones will be, resulting in a blueshift of the vHs. The energy separation ΔE_{vHs} is twist angle (θ) dependent ($\Delta E_{\mathrm{vHs}} = \frac{2}{\sqrt{3}} b\hbar v_{\mathrm{F}}' \sin\left(\frac{\theta}{2}\right) - 2t_\theta$, where b is lattice constant in reciprocal space, v_F' is the renormalized Fermi velocity, and t_θ is the interlayer hopping energy). The experiment results are in agreement with the tight-binding and density functional theory (DFT) calculations.

2.3. Mechanical Coupling: Interlayer Vibrations

The van der Waals coupling affects not only the electronic properties, but also mechanical properties of 2D materials. Raman spectroscopy is a powerful technique to characterize the mechanical coupling between neighboring layers.[58–65] In few-layer graphene, due to its 2D character, the Raman spectrum is usually composed of two dramatically different types of vibrational modes, that is, intralayer and interlayer vibrational modes. The D, G, and 2D peaks are all corresponding to the in-plane intralayer vibrational modes (**Figure 3**b).[65–68] Other peaks in the spectrum, for example, the interlayer shearing modes (C modes) in the in-plane direction and the layer breathing modes (LBMs) in the out-of-plane direction, all originate from the interlayer mechanical coupling (Figure 3a).[69–72] These modes may have slightly different names in other 2D materials, but the vibrational manners are basically similar. Therefore, it is straightforward to use the C modes and LBMs to characterize the interlayer coupling strength.

Compared with G mode in graphene, the C mode is much more sensitive with the stacking layer number. Tan et al.[70] confirmed that the C modes of suspended few-layered graphene range from 31 cm^{-1} for bilayer to 43 cm^{-1} for bulk graphite (Figure 3c). A linear-chain model is proposed to explain this blueshift of C mode from bilayer to bulk graphite: with the layer number increasing, the overall restoring force of the linear-chain increases as well, resulting in a larger shear modulus.

At room temperature, Raman spectrum of LBMs in Bernal stacking multilayer graphene was hardly observed due to its weak electron phonon coupling.[73] While in twist one, LBMs are significantly enhanced under laser excitation energy around

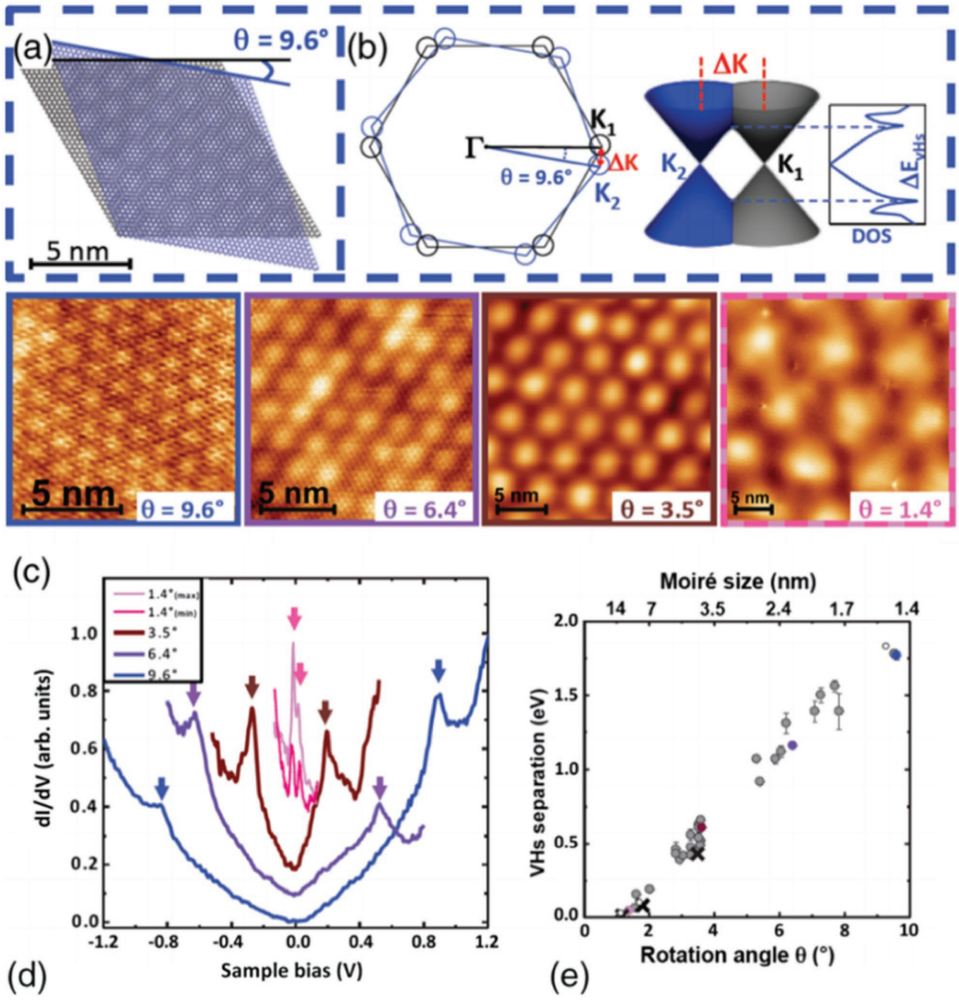

Figure 2. a) Illustration of moiré pattern with twist angle of 9.6°. b) Brillouin zone, energy dispersion relation, and vHs of twisted bilayer graphene. c) Moiré pattern of bilayer graphene with different rotation angle obtained by STM. d) Local DOS spectra taken on the moiré pattern shown in (c). The arrows point to vHs; e) vHs separation as a function of rotation angle. Reproduced with permission.[55] Copyright 2012, American Physical Society.

vHs. Multilayer graphene with different twist angel or number of layers are characterized by low-frequency Raman spectrum and the peak position of LBMs (≈100 cm^{-1}) is found to be determined by the number of stacking layers and independent with twist angle.[74] This indicates the mechanical coupling of graphene is hardly tuned by the stacking orientation between layers.

Because these two interlayer vibration modes directly reflect the collective vibration of component layers, they provide a prototype for investigation of the interlayer interactions in layered materials. LBMs and C modes in TMDCs can be observed significantly even at room temperature due to its strong electron phonon coupling and similar behaviors like graphene are observed in bilayer TMDCs[75–78] and TMDCs heterostructures:[79,80] AA-/AB-stacking bilayers have higher LBM frequency than that in bilayers with arbitrary twist angle, indicating stronger coupling between two layers. While the C mode is absent in twisted bilayers because of the weak in-plane mechanical oscillation strength in incommensurate system.

3. Van der Waals Coupling in Graphene/h-BN Heterostructure

Van der Waals coupling also plays a critical role in determining the properties of van der Waals heterostructure. Graphene/h-BN is a representative example, where the constituent layers, graphene, and h-BN, have dramatically different bandgap (0 eV for graphene, and ≈5.5 eV for h-BN). As a result, the interlayer electronic coupling has distinctively different effects compared to the direct hybridization in bilayer graphene case. In graphene/h-BN heterostructure, the graphene Dirac cones sit deeply within h-BN bandgap, which prevents energy matching between h-BN electronic states and low-energy graphene states. Therefore, the direct coupling between graphene and h-BN electronic states can often be neglected. Instead, the effects of interlayer van der Waals coupling can be modeled with an effective potential on graphene layer, which mixes two electronic states from the same graphene layer.

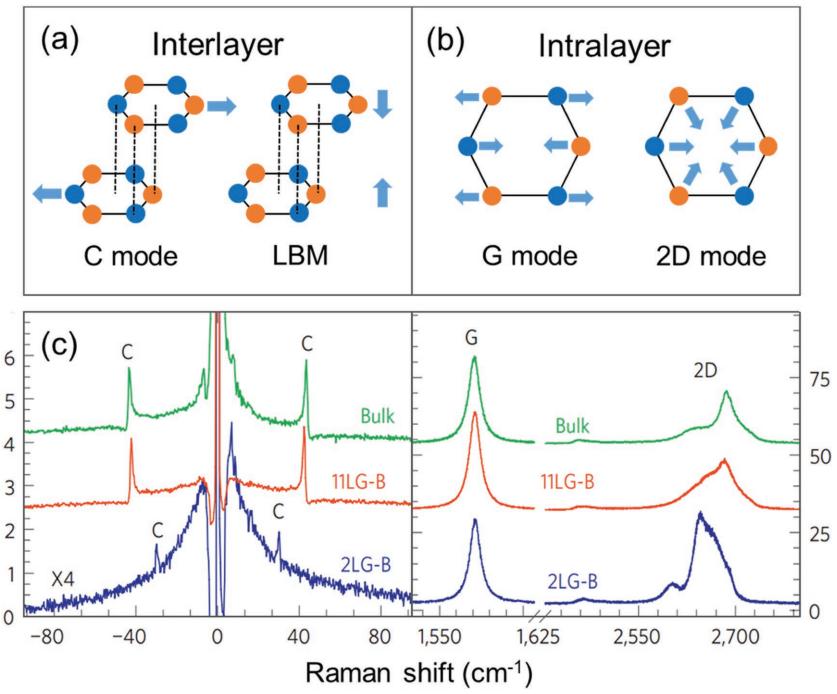

Figure 3. Illustration of a) interlayer and b) intralayer vibrational modes in the examples of C mode, LBM, G mode, and D mode in graphene. c) C mode (left) and G/2D mode (right) spectra of few-layered graphene. The frequency shows layer number dependence. Reproduced with permission.[70] Copyright 2012, Nature Publishing Group.

3.1. Hofstadter's Butterfly in Graphene/h-BN

A fractal energy spectrum is developed when a magnetic field and a superlattice potential are applied simultaneously to an electron system. This spectrum is called the Hofstadter's butterfly. In 2013, the evidence of the Hofstadter's butterfly spectrum was realized in 2D system of graphene/h-BN heterostructure.[81–83] As reported by Dean et al.,[83] graphene/h-BN heterostructure can be fabricated by sequential transfer of individual layers with accurate twist angle control (**Figure 4**a). Since crystal lattices of graphene and h-BN are isomorphic with only 1.8% mismatch, the moiré pattern can have a superlattice periodicity as large as several nanometers, an ideal length scale to explore the fractal spectrum. Figure 4b shows the transport experiment of graphene/h-BN heterostructure, the resistance is measured as a function of the gate voltage, and two extra satellite peaks appeared symmetrically on both sides of the charge neutrality point at temperature 300 mK. But when the temperature rises above 100 K, the two satellite peaks disappear, indicating the weak coupling (≈10 meV) between graphene and h-BN layers. The satellite peaks arise from the secondary Dirac cones, which appear in both conduction and valence bands at the edge of the superlattice Brillouin zone.

As shown in Figure 4c, the periodic potential splits the flat Landau level bands into several "Hofstadter mini-bands." The effects of the superlattice electron potential and the magnetic field to the formation of the mini-band can be described by Wannier's theory: in a magnetic field B, the number of states per area of each filled Landau level is given by B/Φ_0, where $\Phi_0 = h/e$ is the magnetic flux quanta. Energy gaps in the Hofstadter spectrum are constrained by linear trajectories $\Phi/\Phi_0 = (n/n_0 - s)/t$, where $\Phi = B/n_0$ is the magnetic flux per unit cell, where s and t are integers denoting the superlattice mini-band filling index and quantized Hall conductance of the gapped state, respectively. This is different from the usual Landau level description: $\Phi/\Phi_0 = (n/n_0)/\nu$, where ν is the Landau level filling fraction.

3.2. Pseudospin Mixing in Graphene/h-BN Moiré Superlattice

In graphene/h-BN heterostructures, the effective potential on graphene layer should satisfy the symmetry of the system. Therefore, its periodicity is identical to the moiré superlattice of the heterostructure. The simplest potential of such type is a slowly spatially varying scalar potential (because of the large periodicity of moiré superlattice), which was often invoked to understand the emerging mini-Dirac points observed in early transport and STS studies.[81–83] Later it was demonstrated theoretically and experimentally that there were three types of possible potentials satisfying the symmetry of the system, labeled as u_0, u_3, and u_1,[84] with distinctively different physical meaning: u_0 is the slowly varying scalar potential as mentioned above, which cannot open a gap at the boundary of mini-Brillouin zone, and is called "pseudospin-blind" potential. u_3 is spatially varying fast that it becomes opposite at the two graphene sublattices in the same unit cell, and therefore can be called "pseudospin-dependent" potential. u_1 is the "pseudospin-mixing" potential since it does not change potential on specific site, instead it changes the hopping energy between neighboring sublattices. Both u_3 and u_1 terms can open a gap at the boundary of mini-Brillion zone, however the gaps are distinctively different: u_3 opens a "normal" gap and u_1 opens an "inverse" gap, similar to the band inversion phenomena in topological insulators. Optical spectroscopy study reveals the dominant role of u_1, the "pseudospin-mixing" potential, in graphene/h-BN heterostructure, which is consistent with theoretical predictions.[85]

4. Van der Waals Coupling in 2D Materials beyond Graphene

After the discovery of graphene, other atomically thin van der Waals coupled materials, such as infrared-gapped black phosphorus, semiconducting molybdenum disulfide, and insulating h-BN, are developed by directly mechanical exfoliation from their bulk materials or chemical vapor deposition method. These rich 2D materials offer us an extensive platform for studying new physics and engineering next-generation photonics and optoelectronics. In the following section, we will introduce 2D materials beyond graphene, in the examples of black

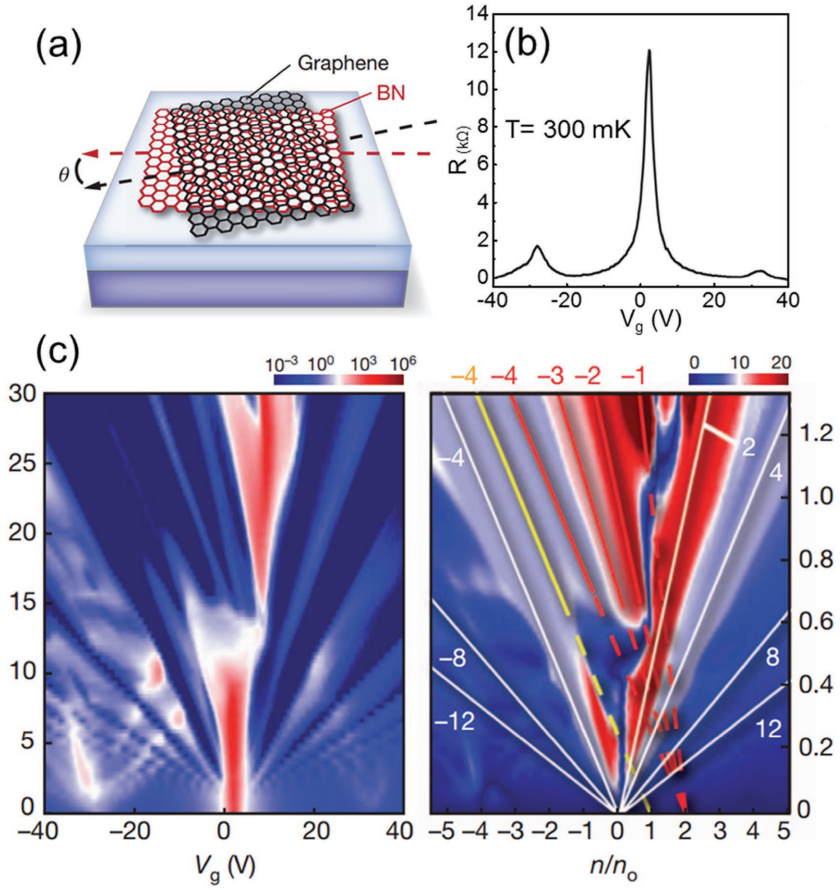

Figure 4. a) Sketch of the layered h-BN and graphene heterostructure with a mismatch angle θ. b) Measured resistance versus gate voltage at temperature of 300 mK with zero magnetic field. The two additional small peaks originated from the sub-Dirac cones caused by the interlayer interactions. c) Landau fan diagram showing longitudinal resistance, R_{xx} (left), and Hall resistance, R_{xy} (right). Reproduced with permission.[83] Copyright 2013, Nature Publishing Group.

phosphorus and TMDCs, and discuss how their properties are tuned by van der Waals coupling between layers.

4.1. Layer-Dependent Electronic Structure in Black Phosphorus

Similar to graphite, black phosphorus is an atomic-layered material with layers stacking together by van der Waals interactions. In the thickness of about 10 nm, black phosphorus exhibits a mobility of 1000 $cm^2\ V^{-1}\ s^{-1}$ at room temperature, which is much higher than that of TMDCs materials.[86–89] In addition, monolayer black phosphorus, that is, phosphorene, is predicted to be a semiconductor with a bandgap of 2 eV at Γ point of its Brillouin zone.[90–94]

The bandgap of few-layer phosphorene decreases continuously as the layer number increases. Theoretical calculations predict that the bandgap of black phosphorus covers a spectrum of 0.3 eV (bulk) to 2 eV (monolayer)[93] which is vital for optoelectronic technologies. PL measurements are used to probe the bandgap of monolayer and few-layer phosphorene but it is affected by the defects and impurities.[87,95–97] Li et al.[98] reported the layer-dependent intrinsic electronic structure in phosphorene by polarization-resolved reflection spectroscopy, which is insensitive to defects and impurities. They reported quantitatively the lowest and above-bandgap higher exciton resonance from monolayer to pentalayer and demonstrated these few-layer phosphorene are all direct bandgap semiconductors. The decrease of bandgap with increasing layer number and the rise of the higher energy exciton resonances are both due to the strong interlayer interactions between layers. These characters can be simply described by 1D tight-binding calculation with considering the coupling of single-particle electronic states at the Γ point in Brillouin zone. Furthermore, the absorption and PL spectra are strongly polarization-dependent as a consequence of highly anisotropic in phosphorene.

4.2. Van der Walls Coupling in Transition Metal Dichalcogenides

The discovery of TMDCs markedly broadens the spectrum of 2D materials and shows many characteristic properties. Most layered TMDCs have bandgaps at visible light energy and undergo an indirect to direct bandgap transition as the thickness is reduced to a monolayer limit.[99,100] Due to the strong light–matter interaction, TMDCs are widely used in optoelectronic and nanophotonic applications.[101–104] The broken inversion symmetry in TMDCs brings about ideal system for exploring spin and valley physics.[105] Therefore, the modulation of those interesting properties through interfacial engineering, namely, the interlayer stacking configuration and applied fields, will be the next popular focus for researchers.

4.2.1. Evolution of Interlayer Coupling in Twisted Bilayer MoS_2

Liu et al.[8] studied the interlayer coupling evolution by Raman and PL spectroscopy. Triangle-shaped MoS_2 monolayers and bilayers with different stacking orders are grown by CVD method. **Figure 5**a shows the PL spectra of monolayer and bilayer MoS_2 with different twist angles. Monolayer MoS_2 shows only one pronounced peak (peak I) resulting from the A exciton recombination at the K point of the Brillouin zone at the energy range <2 eV. For the bilayer case, a lower-energy peak (peak II) arises, which is attributed to an indirect bandgap luminescence between the conduction band states at K and the valence band states at the center of the Brillouin zone (Γ). Here, the valence band splitting at the Γ point plays a critical role in the direct-to-indirect bandgap transition. Due to the van der Waals coupling, the otherwise degenerate valence band states at Γ split into two branches, in which the higher energy branch lies

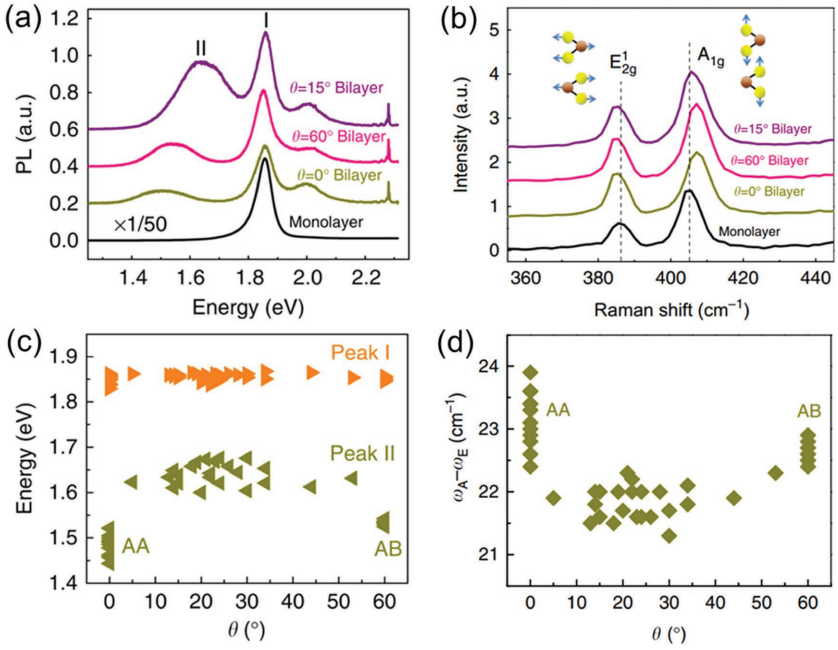

Figure 5. a) PL spectra and b) Raman spectra of MoS_2 monolayer and bilayers with twist angles of 0°, 15°, and 60°. c) The PL peak energy evolution with twist angle, peak I is hardly changed and peak II is lowest for AA-/AB-stacking bilayers. d) Raman peak separation between the A_{1g} and E_{2g} in MoS_2 bilayers of different twist angles, which is the largest for AA or AB stacking and nearly a constant for other twist angles. Reproduced with permission.[8] Copyright 2014, Nature Publishing Group.

at a higher energy than the valence band state at K. Therefore, the indirect bandgap energy (peak II) directly reflects the interlayer coupling strength: the lower the indirect bandgap, the stronger the coupling strength. This is significantly meaningful to determine the correlation of interlayer coupling strength and twist angles configuration. They find the positions of the peak I (direct bandgap transition) are hardly changed with twist angle but peak II turns to much lower energies for perfectly registered, AA-/AB- (twist angle of 0°/60°) stacking MoS_2 bilayers (Figure 5c). This means the interlayer electronic coupling is significant for all twist angles but is strongest in the perfectly registered ones.

The interlayer mechanical coupling of bilayer MoS_2 is studied by Raman spectroscopy (Figure 5b,d). Compared to monolayer MoS_2, the two conspicuous peaks, that is, the in-plane E^1_{2g} and out-of-plane A_{1g} vibration modes, exhibit red and blueshifts, respectively. In particular, the energy shift of the A_{1g} mode, affected by the interlayer mechanical coupling, is strongly dependent on the twist angle. Therefore, the separation between these two peaks $\omega_A - \omega_E$ reflects the effective interlayer mechanical coupling strength: the further the separation, the stronger the coupling strength. Similar to the electronic coupling, the perfect registered bilayers have the strongest mechanical coupling, while for other stacking orders, weaker mechanical coupling is observed.

From ab initio calculations, the interlayer vertical separation has much more crucial effects than the twist angle on the size of the bandgap in van der Waals coupled TMDCs materials. That is different from the gapless graphene, in which the interesting electronic properties around the Dirac point are dramatically modified in small twist angles.

4.2.2. Tunable Valley Polarization in Bilayer MoS_2

Monolayer TMDCs materials have broken inversion symmetry. As a result, the K and K′ valleys are no longer equivalent. Interband transitions at those two valleys should follow the valley-selective circular dichroism.[105–109] At the K valley, only light of right (σ+) circular polarization can be absorbed, whereas at the K′ valley, only light of left (σ–) circular polarization can be absorbed. In AB-stacking bilayer TMDCs materials, the inversion symmetry is preserved and the valley-selective circular dichroism vanishes, while the circular dichroism can be reinstated by changing the stacking configuration[9,110] between the two layers, or using an electric field[11,111] to break the inversion symmetry.

Jiang et al.[9] found the robust valley and spin polarization in twisted MoS_2 bilayer. This is much different from the naturally stacking bilayer, because the inversion symmetry is broken in twisted bilayers and the valley-selective circular dichroism is allowed. Furthermore, the interlayer coupling is largely reduced compared to that of naturally stacking bilayer. It means that the twisted bilayer MoS_2 is more similar to "doubled monolayer." As a result, the spin configuration is locked in individual layers, leading to the observation of valley polarization.

The inversion symmetry of AB-stacked bilayer MoS_2 can also be broken by applying a perpendicular electronic field similar to that in Bernal stacking bilayer graphene. Wu et al.[11] reported the valley magnetic moments in bilayer MoS_2 are tunable by applying a perpendicular electronic filed, and the potential difference between two layers leads to the inversion symmetry broken. A back-gate voltage V_g was applied to control the electric field in field-effect transistors. They found that the degree of polarization depends strongly on the back-gate voltage and approaches zero at a certain voltage V_c. In further investigation, they found the absolute value of the degree of polarization is symmetric when tuning V_g around V_c, and saturates when $|V_g\text{-}V_c| \gtrsim 30$ V. In comparison, the polarization from monolayer MoS_2 under the same condition is gate independent.

4.3. TMDCs Heterojunction

Heterojunctions stacked by atomically thin van der Waals materials provide a different approach of materials engineering through modifying the interlayer interactions. These heterojunctions can be simply obtained from transfer[47,112–115] and CVD method.[116–120] Most of the monolayer TMDCs are direct bandgap semiconductor showing strong light–matter

interaction.[121–123] However, according to theoretical calculations, when these monolayers stack vertically and form heterojunctions, many of these heterojunctions have type II band alignment,[124–127] which means the conduction band minimum and valence band maximum reside in two different layers. Therefore, the photoexcited electrons and holes can naturally separate into the two different layers.[128–132] Those separated electrons and holes are still bound by Coulomb interaction due to the strong spatial confinement and reduced screening effects compared to bulk solids, and those pairs are often referred to as interlayer excitons.[133,134] These TMDCs heterostructures provide an ideal platform for investigating new physics and are regarded as candidates for optoelectronic devices such as photodiodes, photovoltaic cells, and light-emitting devices.

4.3.1. Ultrafast Charge Transfer

Hong et al.[128] first reported the ultrafast charge transfer in MoS_2/WS_2 heterostructure prepared by transfer methods. The band alignment is schematically shown in **Figure 6**a. In the PL spectra, the MoS_2 and WS_2 monolayers show strong intensities at their respective A-exciton resonances, while signals are efficiently quenched in the MoS_2/WS_2 heterostructure because of the ultrafast interlayer charge transfer. To detect the charge transfer process, transient absorption spectroscopy measurement was performed by pump–probe technique at 77 K. A femtosecond pulse was used to excite the A-exciton of MoS_2 with a pump laser energy low enough to avoid exciting the A-exciton of WS_2. Then the photoinduced changes in the reflection spectra ($\Delta R/R$), which is directly proportional to the change in absorption coefficient, are probed by a supercontinuum femtosecond pulse after controlled time delays. Therefore, the accumulation of electrons and holes in different layers can be detected by a probe light with proper wavelength. Figure 6b presents a 2D plot of transient absorption spectrum in a MoS_2/WS_2 heterostructure as a function of time-delay and probe energy at 77 K. A significant peak can be observed around 2.059 eV, corresponding to the WS_2 A-exciton resonance in MoS_2/WS_2 heterostructure. Since the pump laser energy (1.86 eV) is much lower than WS_2 A-exciton resonance energy, this signal must be related to the hole transfer from MoS_2 to WS_2. The hole transfer time is determined to be ultrafast (sub-50 fs) in this weakly coupled MoS_2/WS_2 heterostructure, after deconvolution of the transient absorption signals (Figure 6c).

4.3.2. Valley-Polarized Interlayer Excitons

Rivera et al.[133] detected the interlayer exciton luminescence signal in $MoSe_2/WSe_2$ heterostructure, in which the electrons and holes locate at different layers. The lifetime of these interlayer excitons is as long as 1.8 ns, much longer than that of interlayer excitons in monolayers. Recently, they found this interlayer excitons can be spin-valley polarized similar to that of a monolayer.[135] The heterostructures consist of exfoliated monolayers of WSe_2 and $MoSe_2$, which are aligned with twist angle near 0°, and the Brillouin zones of the two layers are almost perfectly overlapped (**Figure 7**a). As we have discussed above, $MoSe_2/WSe_2$ heterostructures have type II band alignment as shown in Figure 7b. Under excitation of light, ultrafast charge transfer takes place and the interlayer excitons form. A factor $\rho = \frac{I_+ - I_-}{I_+ + I_-}$ is defined to describe the degree of polarization. $I_\pm$ is the intensity of PL with right or left circularly polarization. When a right circularly polarized (σ^+) laser excite, the interlayer exciton PL intensity of σ^+ and σ^- are detected, as shown in Figure 7c. The data reflect the interlayer exciton is valley-polarized with a degree of the polarization greater than 0.3. Time-resolved interlayer exciton PL measurement was carried out to study the decay of valley polarization and found the valley polarization can remain in nanoseconds (Figure 7d).

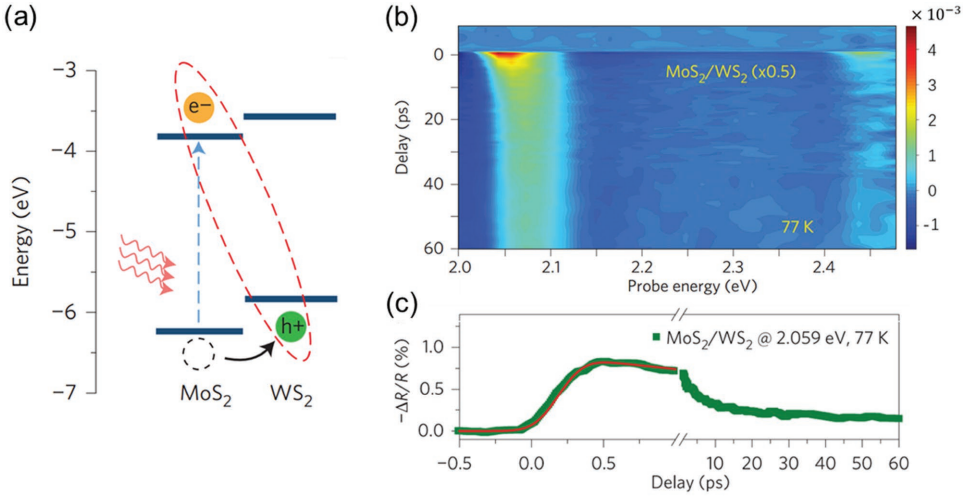

Figure 6. a) Band alignment of MoS_2/WS_2 heterostructure from theoretical calculation. The hole in laser excited MoS_2 will transfer to a lower energy at WS_2 layer, forming interlayer exciton. b) 2D plots of transient absorption spectra at 77 K from a MoS_2/WS_2 heterostructure under pump energy of 1.86 eV. The significant peak around 2.059 eV is corresponding to the resonance of WS_2 A-exciton. c) Dynamic evolution of transient absorption signal at the WS_2 A-exciton resonance in the MoS_2/WS_2 heterostructure. After deconvolution, the hole transfer between layers is determined to be ultrafast, within 50 fs. Reproduced with permission.[128] Copyright 2014, Nature Publishing Group.

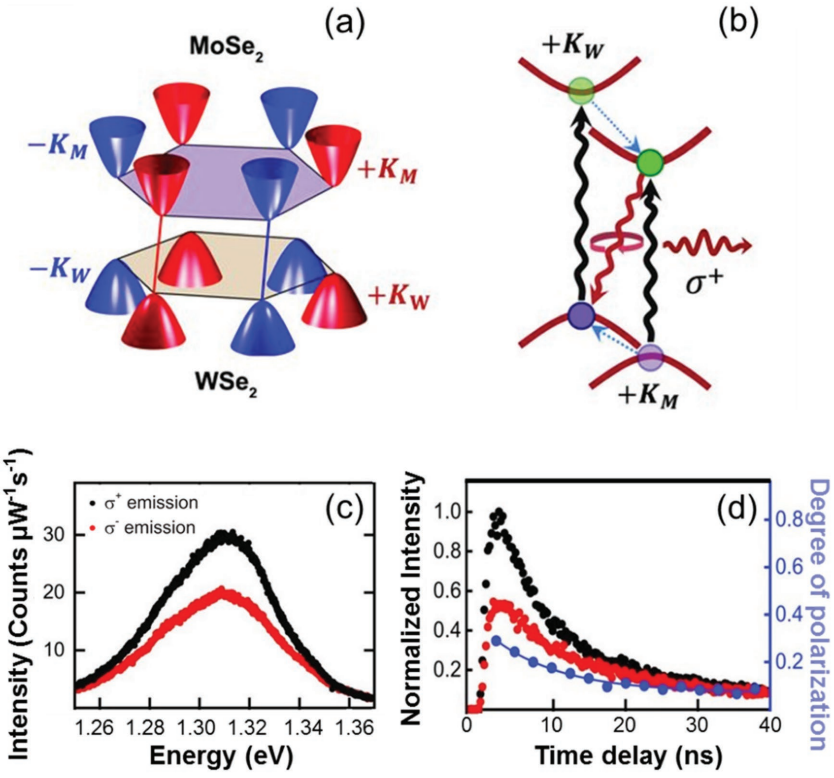

Figure 7. a) Brillouin zone of a $MoSe_2$-WSe_2 heterostructure, with twist angle near zero. b,c) Schematic and PL spectra of valley-polarized exciton. With σ+ circularly polarized light excited, the interlayer exciton mainly have σ+ circularly polarized luminescence. d) Time-resolved interlayer exciton PL shows long-lived interlayer exciton with polarization. Reproduced with permission.[135] Copyright 2016, American Association for the Advancement of Science.

These long-lived valley-polarized interlayer excitons exhibit lateral drift and diffusion over several micrometers.

5. Applications Based on Van der Waals Coupled 2D Materials

We have discussed about the physical properties in layered materials engineered by the van der Waals interaction hereinbefore. In addition, this interaction is believed to be an effective method to combine various properties in a single device. Such concept leads us to realize fruitful photonics and optoelectronics applications with amazing performance.

Vertical stacking heterostructure of graphene and TMDCs is considered to be an ideal photodetector with high efficiency and ultrafast photoresponse. In this kind of 2D photodetectors, there are three main processes in the photocurrent generation: light absorption to form excitons, excitons dissociation to free electron–hole pairs, and the electron hole transfer to positive and negative electrodes. In this system, TMDCs have strong light–matter interaction, and 95% of the light across the visible range can be absorbed by a 300 nm thin film,[18,136] while graphene is regarded as transparent and flexible electrode due to its high mobility.[137–140] As the channel in this heterostructure device can be as short as few nanometers, large enough electrical field can be applied to direct the strongly bound electrons and holes to move in opposite directions (approximately hundred meV).[141–145] At the same time, the efficient and ultrafast charge separation between TMDCs and graphene layers leads to a high quantum efficiency and ultrafast photoresponse in the heterostructure device.[128,146]

Graphene/TMDCs/graphene vertical photodetector with h-BN encapsulated were fabricated by Britnell et al.[18] Two pieces of monolayer graphene are used as source and drain electrodes with gate-tunable work-functions. The intercalary few-layer WSe_2 serves as photoactive material. As shown in **Figure 8**a, when a gate voltage is applied, photoexcited electron–hole pairs in WSe_2 will separate into the upper and lower graphene layers, respectively. The external quantum efficiency, defined as the ratio of the number of generated charge carriers to the number of incident photons, is demonstrated to be as high as 30%. In the further work of Massicotte et al.,[147] the photoresponse time is determined to be as fast as ≈5 ps, detected by time-resolved photocurrent measurements (Figure 8b).

6. Discussion

As discussed in Section 2, the interlayer electronic coupling in van der Waals systems has two types: "direct hybridization" in systems like bilayer graphene, bilayer MoS_2, etc.; and "effective potential" in systems like graphene/h-BN. These two situations are quite different.

In the direct hybridization case, giving a specific electronic state in one layer (state 1), the momentum selection rules require that only states in the other layer with the same momentum (state 2) can directly couple to it. Note that here "same" is comparing to a shared reference frame, for example, the Brillouin zone of layer 1 (BZ1). Depending on the interlayer alignment, state 2 will be different states compared to BZ2, since BZ2 and BZ1 can be aligned differently. If the energy of state 2 matches with state 1, that is, degenerate coupling case, the coupling will be particularly strong, often leading to new features, such as vHs in bilayer graphene. Therefore, the momentum and energy of degenerately coupled states will sensitively depend on twist angle, and can be simply determined by overlaying the band structures of two layers and find the crossing points.

One unique example is states with zero momentum (Γ point), since the momentum selection rule always allows them to couple to others states at Γ point. If the two layers are the same material, Γ point states always have the same energy, regardless of interlayer twist angle. Therefore, in systems such as bilayer MoS_2 with arbitrary twist angle, the Γ point states always have strong coupling and split into two, making bilayer MoS_2 an indirect bandgap semiconductor. The

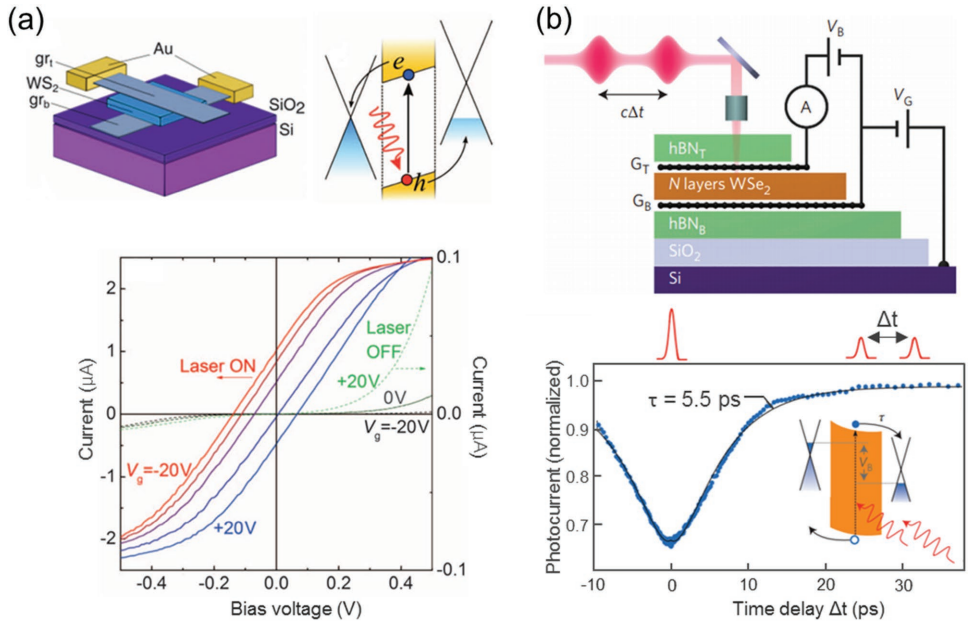

Figure 8. a) Top left: WS_2 photovoltaic devices with two graphene layers as transparent electrodes. Top right: Band alignment with a built-in electric field. Excitons in WS_2 dissociate to free electron–hole pairs and transfer to graphene electrodes. Bottom: Current as a function of bias voltage with and without light illumination. Reproduced with permission.[18] Copyright 2013, American Association for the Advancement of Science. b) Top: Schematic illustrating the cross-sectional view of the h-BN/G/WSe_2/G/h-BN heterostructure device. The time-resolved photocurrent was detected as two ultrashort pulse lasers with a time-delay Δt focused on the device. Bottom: Time-resolved photocurrent measurements results, from the rise curve we can get the response time of the device, $\tau = 5.5$ ps. Reproduced with permission.[147] Copyright 2015, Nature Publishing Group.

shearing mode or layer-breathing Raman mode also refers to the Γ point. In bilayer MoS_2, the coupling strength only depends explicitly on the interlayer spacing rather than twist angle. This scenario changes in materials systems with anisotropy, where the interlayer coupling at Γ point can depend strongly on the interlayer twist angle. For example, in bilayer black phosphorus, theoretical calculations show that the coupling between the valence band tops of the two layers vanishes as the twist angle approaches 90°, while such coupling is quite strong and splits the two band tops by around 1 eV at 0° twist angle.[148]

In the effective potential case, momentum selection rule still exists, however the exact form is completely different. The momentum conservation requires that any two states can be coupled if their momentum difference is the same, and therefore can be compensated by Umklapp scattering, that is, the momentum of the effective potential, $q_{n_1,n_2,m_1,m_2} = n_1\, b_{11} + n_2 b_{12} + m_1 b_{21} + m_2 b_{22}$, where b_{1j} and b_{2j} are reciprocal lattice vectors of layer 1 and layer 2. Usually the Fourier component amplitude of the effective potential with momentum q decreases very fast with $|q|$, and therefore only a few terms need to be considered. Taking graphene/h-BN heterostructure with small twist angle as an example, since b_{1j} and b_{2j} are close, we can let $n_1 = -m_1$ and $n_2 = -m_2$ to minimize $|q|$. Then we get $q_{n_1,n_2} = n_1\,(b_{11} - b_{21}) + n_2(b_{12} - b_{22}) = n_1\, c_1 + n_2 c_2$, where c_1 and c_2 are reciprocal lattice vectors of the mini-Brillouin zone. And the selection rule requires that states at boundary of the mini-Brillouin zone will have degenerate coupling, as has been discussed in various studies.[84,149,150]

7. Conclusion

In this paper, we review recent progress in the interfacial engineering of a number of 2D layered material systems, including bilayer graphene, graphene/h-BN heterostructures, bilayer TMDCs, and TMDCs heterostructures. In these systems, the interfacial engineering, which is realized by changing the stacking configuration and/or applying external fields, leads to material properties different from neither a monolayer system nor a bulk system. We further elucidate the origins of these changes, and discuss the essential role of the modification of the interlayer coupling.

This interfacial engineering of van der Waals coupled 2D layered materials has been rapidly expanding the breadth of the 2D materials research, since the van der Waals coupled layers can virtually be achieved by stacking any kind of 2D materials together and host a great platform for studying a wide range of physical phenomena in these systems. However, the industrial applications of these coupled layers still have a way to go, because the large-scale and controlled synthesis of van der Waals coupled 2D materials of predesigned stacking is still of great challenge. At the current stage, the usual mechanical transfer method is inefficient and labor-intensive. Also, the size of fabricated samples is mostly in micrometer scale, far away from the wafer-scale size as needed in industry. These factors all limit the immediate application of these materials in the modern industry.

We would also like to point out a few unsolved problems and opportunities in the interfacial engineering of 2D materials. The first problem is an unclear understanding of the dynamical

process in van der Waals coupled layers, such as the ultrafast charge and energy transfer, phonon dynamics, and photocurrent generation. The understanding of these dynamical processes is important for rational design of future electronic and optoelectronic devices. More works should be performed to explore the relations between the interfacial structure and the ultrafast process. The second issue is to use interfacial engineering to study other novel phenomena beyond the electronic and optical ones. As recent studies have demonstrated that 2D materials could develop ferromagnetism and superconductivity, it is quite natural to ask whether these properties can be controlled by interlayer engineering methods introduced in this review.

Acknowledgements

H.H., C.L., and T.C. contributed equally to this work. This work was supported by National Key R&D Program of China (2016YFA0300903), National Natural Science Foundation of China (NSFC) (51522201, 11474006, and 91433102), the National Program for Thousand Young Talents of China, and National Science Foundation of USA (NSF) (DMR-1404865).

Received: November 2, 2016
Revised: December 29, 2016
Published online:

[1] K. S. Novoselov, D. Jiang, F. Schedin, T. J. Booth, V. V. Khotkevich, S. V. Morozov, A. K. Geim, *Proc. Natl. Acad. Sci. USA* **2005**, *102*, 10451.
[2] K. S. Novoselov, A. K. Geim, S. V. Morozov, D. Jiang, M. I. Katsnelson, I. V. Grigorieva, S. V. Dubonos, A. A. Firsov, *Nature* **2005**, *438*, 197.
[3] Y. B. Zhang, Y. W. Tan, H. L. Stormer, P. Kim, *Nature* **2005**, *438*, 201.
[4] A. K. Geim, K. S. Novoselov, *Nat. Mater.* **2007**, *6*, 183.
[5] Q. H. Wang, K. Kalantar-Zadeh, A. Kis, J. N. Coleman, M. S. Strano, *Nat. Nanotechnol.* **2012**, *7*, 699.
[6] A. K. Geim, I. V. Grigorieva, *Nature* **2013**, *499*, 419.
[7] G. Li, A. Luican, J. M. B. Lopes dos Santos, A. H. Castro Neto, A. Reina, J. Kong, E. Y. Andrei, *Nat. Phys.* **2009**, *6*, 109.
[8] K. H. Liu, L. M. Zhang, T. Cao, C. H. Jin, D. A. Qiu, Q. Zhou, A. Zettl, P. D. Yang, S. G. Louie, F. Wang, *Nat. Commun.* **2014**, *5*, 4966.
[9] T. Jiang, H. R. Liu, D. Huang, S. Zhang, Y. G. Li, X. G. Gong, Y. R. Shen, W. T. Liu, S. W. Wu, *Nat. Nanotechnol.* **2014**, *9*, 825.
[10] Y. Zhang, T. T. Tang, C. Girit, Z. Hao, M. C. Martin, A. Zettl, M. F. Crommie, Y. R. Shen, F. Wang, *Nature* **2009**, *459*, 820.
[11] S. F. Wu, J. S. Ross, G. B. Liu, G. Aivazian, A. Jones, Z. Y. Fei, W. G. Zhu, D. Xiao, W. Yao, D. Cobden, X. D. Xu, *Nat. Phys.* **2013**, *9*, 149.
[12] L. Britnell, R. V. Gorbachev, R. Jalil, B. D. Belle, F. Schedin, A. Mishchenko, T. Georgiou, M. I. Katsnelson, L. Eaves, S. V. Morozov, N. M. R. Peres, J. Leist, A. K. Geim, K. S. Novoselov, L. A. Ponomarenko, *Science* **2012**, *335*, 947.
[13] H. Yang, J. Heo, S. Park, H. J. Song, D. H. Seo, K. E. Byun, P. Kim, I. Yoo, H. J. Chung, K. Kim, *Science* **2012**, *336*, 1140.
[14] T. Georgiou, R. Jalil, B. D. Belle, L. Britnell, R. V. Gorbachev, S. V. Morozov, Y. J. Kim, A. Gholinia, S. J. Haigh, O. Makarovsky, L. Eaves, L. A. Ponomarenko, A. K. Geim, K. S. Novoselov, A. Mishchenko, *Nat. Nanotechnol.* **2013**, *8*, 100.
[15] M. M. Furchi, A. Pospischil, F. Libisch, J. Burgdorfer, T. Mueller, *Nano Lett.* **2014**, *14*, 4785.
[16] M. Fontana, T. Deppe, A. K. Boyd, M. Rinzan, A. Y. Liu, M. Paranjape, P. Barbara, *Sci. Rep.* **2013**, *3*, 1634.
[17] J. S. Ross, P. Klement, A. M. Jones, N. J. Ghimire, J. Q. Yan, D. G. Mandrus, T. Taniguchi, K. Watanabe, K. Kitamura, W. Yao, D. H. Cobden, X. D. Xu, *Nat. Nanotechnol.* **2014**, *9*, 268.
[18] L. Britnell, R. M. Ribeiro, A. Eckmann, R. Jalil, B. D. Belle, A. Mishchenko, Y. J. Kim, R. V. Gorbachev, T. Georgiou, S. V. Morozov, A. N. Grigorenko, A. K. Geim, C. Casiraghi, A. H. Castro Neto, K. S. Novoselov, *Science* **2013**, *340*, 1311.
[19] W. J. Yu, Y. Liu, H. L. Zhou, A. X. Yin, Z. Li, Y. Huang, X. F. Duan, *Nat. Nanotechnol.* **2013**, *8*, 952.
[20] F. Withers, O. Del Pozo-Zamudio, A. Mishchenko, A. P. Rooney, A. Gholinia, K. Watanabe, T. Taniguchi, S. J. Haigh, A. K. Geim, A. I. Tartakovskii, K. S. Novoselov, *Nat. Mater.* **2015**, *14*, 301.
[21] K. H. Liu, X. P. Hong, M. H. Wu, F. J. Xiao, W. L. Wang, X. D. Bai, J. W. Ager, S. Aloni, A. Zettl, E. G. Wang, F. Wang, *Nat. Commun.* **2013**, *4*, 1375.
[22] K. H. Liu, C. H. Jin, X. P. Hong, J. Kim, A. Zettl, E. G. Wang, F. Wang, *Nat. Phys.* **2014**, *10*, 737.
[23] A. H. Castro Neto, F. Guinea, N. M. R. Peres, K. S. Novoselov, A. K. Geim, *Rev. Mod. Phys.* **2009**, *81*, 109.
[24] A. K. Geim, *Science* **2009**, *324*, 1530.
[25] M. J. Allen, V. C. Tung, R. B. Kaner, *Chem. Rev.* **2010**, *110*, 132.
[26] X. Huang, Z. Y. Yin, S. X. Wu, X. Y. Qi, Q. Y. He, Q. C. Zhang, Q. Y. Yan, F. Boey, H. Zhang, *Small* **2011**, *7*, 1876.
[27] I. W. Frank, D. M. Tanenbaum, A. M. Van der Zande, P. L. McEuen, *J. Vac. Sci. Technol., B* **2007**, *25*, 2558.
[28] C. Lee, X. D. Wei, J. W. Kysar, J. Hone, *Science* **2008**, *321*, 385.
[29] J. N. Grima, S. Winczewski, L. Mizzi, M. C. Grech, R. Cauchi, R. Gatt, D. Attard, K. W. Wojciechowski, J. Rybicki, *Adv. Mater.* **2015**, *27*, 1455.
[30] A. A. Balandin, S. Ghosh, W. Z. Bao, I. Calizo, D. Teweldebrhan, F. Miao, C. N. Lau, *Nano Lett.* **2008**, *8*, 902.
[31] W. W. Cai, A. L. Moore, Y. W. Zhu, X. S. Li, S. S. Chen, L. Shi, R. S. Ruoff, *Nano Lett.* **2010**, *10*, 1645.
[32] A. A. Balandin, *Nat. Mater.* **2011**, *10*, 569.
[33] X. F. Xu, L. F. C. Pereira, Y. Wang, J. Wu, K. W. Zhang, X. M. Zhao, S. Bae, C. T. Bui, R. G. Xie, J. T. L. Thong, B. H. Hong, K. P. Loh, D. Donadio, B. W. Li, B. Ozyilmaz, *Nat. Commun.* **2014**, *5*, 3689.
[34] A. B. Kuzmenko, E. van Heumen, F. Carbone, D. van der Marel, *Phys. Rev. Lett.* **2008**, *100*, 117401.
[35] F. Bonaccorso, Z. Sun, T. Hasan, A. C. Ferrari, *Nat. Photonics* **2010**, *4*, 611.
[36] K. F. Mak, L. Ju, F. Wang, T. F. Heinz, *Solid State Commun.* **2012**, *152*, 1341.
[37] D. N. Basov, M. M. Fogler, A. Lanzara, F. Wang, Y. B. Zhang, *Rev. Mod. Phys.* **2014**, *86*, 959.
[38] S. Lee, K. Lee, Z. H. Zhong, *Nano Lett.* **2010**, *10*, 4702.
[39] W. Liu, S. Kraemer, D. Sarkar, H. Li, P. M. Ajayan, K. Banerjeet, *Chem. Mater.* **2014**, *26*, 907.
[40] W. J. Fang, A. L. Hsu, Y. Song, A. G. Birdwell, M. Amani, M. Dubey, M. S. Dresselhaus, T. Palacios, J. Kong, *ACS Nano* **2014**, *8*, 6491.
[41] V. L. Nguyen, D. J. Perello, S. Lee, C. T. Nai, B. G. Shin, J. G. Kim, H. Y. Park, H. Y. Jeong, J. Zhao, Q. A. Vu, S. H. Lee, K. P. Loh, S. Y. Jeong, Y. H. Lee, *Adv. Mater.* **2016**, *28*, 8177.
[42] Y. F. Hao, L. Wang, Y. Y. Liu, H. Chen, X. H. Wang, C. Tan, S. Nie, J. W. Suk, T. F. Jiang, T. F. Liang, J. F. Xiao, W. J. Ye, C. R. Dean, B. I. Yakobson, K. F. McCarty, P. Kim, J. Hone, L. Colombo, R. S. Ruoff, *Nat. Nanotechnol.* **2016**, *11*, 426.
[43] X. Z. Xu, C. F. Lin, R. Fu, S. Wang, R. Pan, G. S. Chen, Q. X. Shen, C. Liu, X. Guo, Y. Q. Wang, R. G. Zhao, K. H. Liu, Z. T. Luo, Z. H. Hu, H. Y. Li, *AIP Adv.* **2016**, *6*, 025026.

[44] J. B. Oostinga, H. B. Heersche, X. L. Liu, A. F. Morpurgo, L. M. K. Vandersypen, *Nat. Mater.* **2008**, *7*, 151.
[45] K. F. Mak, C. H. Lui, J. Shan, T. F. Heinz, *Phys. Rev. Lett.* **2009**, *102*, 256405.
[46] F. N. Xia, D. B. Farmer, Y. M. Lin, P. Avouris, *Nano Lett.* **2010**, *10*, 715.
[47] A. Castellanos-Gomez, M. Buscema, R. Molenaar, V. Singh, L. Janssen, H. S. J. van der Zant, G. A. Steele, *2D Mater.* **2014**, *1*, 011002.
[48] L. Banszerus, M. Schmitz, S. Engels, J. Dauber, M. Oellers, F. Haupt, K. Watanabe, T. Taniguchi, B. Beschoten, C. Stampfer, *Sci. Adv.* **2015**, *1*, e1500222.
[49] T. Ohta, A. Bostwick, T. Seyller, K. Horn, E. Rotenberg, *Science* **2006**, *313*, 951.
[50] J. M. B. L. dos Santos, N. M. R. Peres, A. H. Castro, *Phys. Rev. Lett.* **2007**, *99*, 216802.
[51] G. T. de Laissardiere, D. Mayou, L. Magaud, *Nano Lett.* **2010**, *10*, 804.
[52] R. Bistritzer, A. H. MacDonald, *Proc. Natl. Acad. Sci. USA* **2011**, *108*, 12233.
[53] P. San-Jose, J. Gonzalez, F. Guinea, *Phys. Rev. Lett.* **2012**, *108*, 216802.
[54] W. Yan, M. X. Liu, R. F. Dou, L. Meng, L. Feng, Z. D. Chu, Y. F. Zhang, Z. F. Liu, J. C. Nie, L. He, *Phys. Rev. Lett.* **2012**, *109*, 126801.
[55] I. Brihuega, P. Mallet, H. Gonzalez-Herrero, G. T. de Laissardiere, M. M. Ugeda, L. Magaud, J. M. Gomez-Rodriguez, F. Yndurain, J. Y. Veuillen, *Phys. Rev. Lett.* **2012**, *109*, 196802.
[56] K. Kim, S. Coh, L. Z. Tan, W. Regan, J. M. Yuk, E. Chatterjee, M. F. Crommie, M. L. Cohen, S. G. Louie, A. Zettl, *Phys. Rev. Lett.* **2012**, *108*, 246103.
[57] R. W. Havener, H. Zhuang, L. Brown, R. G. Hennig, J. Park, *Nano Lett.* **2012**, *12*, 3162.
[58] X. Ling, L. B. Liang, S. X. Huang, A. A. Puretzky, D. B. Geohegan, B. G. Sumpter, J. Kong, V. Meunier, M. S. Dresselhaus, *Nano Lett.* **2015**, *15*, 4080.
[59] X. Lu, M. I. B. Utama, J. H. Lin, X. Luo, Y. Y. Zhao, J. Zhang, S. T. Pantelides, W. Zhou, S. Y. Quek, Q. H. Xiong, *Adv. Mater.* **2015**, *27*, 4502.
[60] G. Froehlicher, E. Lorchat, F. Fernique, C. Joshi, A. Molina-Sanchez, L. Wirtz, S. Berciaud, *Nano Lett.* **2015**, *15*, 6481.
[61] J. U. Lee, J. Park, Y. W. Son, H. Cheong, *Nanoscale* **2015**, *7*, 3229.
[62] A. A. Puretzky, L. B. Liang, X. F. Li, K. Xiao, K. Wang, M. Mahjouri-Samani, L. Basile, J. C. Idrobo, B. G. Sumpter, V. Meunier, D. B. Geohegan, *ACS Nano* **2015**, *9*, 6333.
[63] Y. Y. Zhao, X. Luo, J. Zhang, J. X. Wu, X. X. Bai, M. X. Wang, J. F. Jia, H. L. Peng, Z. F. Liu, S. Y. Quek, Q. H. Xiong, *Phys. Rev. B* **2014**, *90*, 245428.
[64] R. He, J. A. Yan, Z. Y. Yin, Z. P. Ye, G. H. Ye, J. Cheng, J. Li, C. H. Lui, *Nano Lett.* **2016**, *16*, 1404.
[65] A. C. Ferrari, J. C. Meyer, V. Scardaci, C. Casiraghi, M. Lazzeri, F. Mauri, S. Piscanec, D. Jiang, K. S. Novoselov, S. Roth, A. K. Geim, *Phys. Rev. Lett.* **2006**, *97*, 187401.
[66] A. C. Ferrari, *Solid State Commun.* **2007**, *143*, 47.
[67] A. Das, S. Pisana, B. Chakraborty, S. Piscanec, S. K. Saha, U. V. Waghmare, K. S. Novoselov, H. R. Krishnamurthy, A. K. Geim, A. C. Ferrari, A. K. Sood, *Nat. Nanotechnol.* **2008**, *3*, 210.
[68] L. M. Malard, M. A. Pimenta, G. Dresselhaus, M. S. Dresselhaus, *Phys. Rep* **2009**, *473*, 51.
[69] C. H. Lui, L. M. Malard, S. Kim, G. Lantz, F. E. Laverge, R. Saito, T. F. Heinz, *Nano Lett.* **2012**, *12*, 5539.
[70] P. H. Tan, W. P. Han, W. J. Zhao, Z. H. Wu, K. Chang, H. Wang, Y. F. Wang, N. Bonini, N. Marzari, N. Pugno, G. Savini, A. Lombardo, A. C. Ferrari, *Nat. Mater.* **2012**, *11*, 294.
[71] C. H. Lui, T. F. Heinz, *Phys. Rev. B* **2013**, *87*, 121404.
[72] J. B. Wu, X. Zhang, M. Ijas, W. P. Han, X. F. Qiao, X. L. Li, D. S. Jiang, A. C. Ferrari, P. H. Tan, *Nat. Commun.* **2014**, *5*, 5309.
[73] C. H. Lui, Z. P. Ye, C. Keiser, X. Xiao, R. He, *Nano Lett.* **2014**, *14*, 4615.
[74] J. B. Wu, Z. X. Hu, X. Zhang, W. P. Han, Y. Lu, W. Shi, X. F. Qiao, M. Ijias, S. Milana, W. Ji, A. C. Ferrari, P. H. Tan, *ACS Nano* **2015**, *9*, 7440.
[75] X. Zhang, W. P. Han, J. B. Wu, S. Milana, Y. Lu, Q. Q. Li, A. C. Ferrari, P. H. Tan, *Phys. Rev. B* **2013**, *87*, 115413.
[76] Y. Zhao, X. Luo, H. Li, J. Zhang, P. T. Araujo, C. K. Gan, J. Wu, H. Zhang, S. Y. Quek, M. S. Dresselhaus, Q. Xiong, *Nano Lett.* **2013**, *13*, 1007.
[77] S. X. Huang, L. B. Liang, X. Ling, A. A. Puretzky, D. B. Geohegan, B. G. Sumpter, J. Kong, V. Meunier, M. S. Dresselhaus, *Nano Lett.* **2016**, *16*, 1435.
[78] A. A. Puretzky, L. B. Liang, X. F. Li, K. Xiao, B. G. Sumpter, V. Meunier, D. B. Geohegan, *ACS Nano* **2016**, *10*, 2736.
[79] C. H. Lui, Z. P. Ye, C. Ji, K. C. Chiu, C. T. Chou, T. I. Andersen, C. Means-Shively, H. Anderson, J. M. Wu, T. Kidd, Y. H. Lee, R. He, *Phys. Rev. B* **2015**, *91*, 165403.
[80] J. Zhang, J. H. Wang, P. Chen, Y. Sun, S. Wu, Z. Y. Jia, X. B. Lu, H. Yu, W. Chen, J. Q. Zhu, G. B. Xie, R. Yang, D. X. Shi, X. L. Xu, J. Y. Xiang, K. H. Liu, G. Y. Zhang, *Adv. Mater.* **2016**, *28*, 1950.
[81] B. Hunt, J. D. Sanchez-Yamagishi, A. F. Young, M. Yankowitz, B. J. LeRoy, K. Watanabe, T. Taniguchi, P. Moon, M. Koshino, P. Jarillo-Herrero, R. C. Ashoori, *Science* **2013**, *340*, 1427.
[82] L. A. Ponomarenko, R. V. Gorbachev, G. L. Yu, D. C. Elias, R. Jalil, A. A. Patel, A. Mishchenko, A. S. Mayorov, C. R. Woods, J. R. Wallbank, M. Mucha-Kruczynski, B. A. Piot, M. Potemski, I. V. Grigorieva, K. S. Novoselov, F. Guinea, V. I. Fal'ko, A. K. Geim, *Nature* **2013**, *497*, 594.
[83] C. R. Dean, L. Wang, P. Maher, C. Forsythe, F. Ghahari, Y. Gao, J. Katoch, M. Ishigami, P. Moon, M. Koshino, T. Taniguchi, K. Watanabe, K. L. Shepard, J. Hone, P. Kim, *Nature* **2013**, *497*, 598.
[84] Z. W. Shi, C. H. Jin, W. Yang, L. Ju, J. Horng, X. B. Lu, H. A. Bechtel, M. C. Martin, D. Y. Fu, J. Q. Wu, K. Watanabe, T. Taniguchi, Y. B. Zhang, X. D. Bai, E. G. Wang, G. Y. Zhang, F. Wang, *Nat. Phys.* **2014**, *10*, 743.
[85] D. S. L. Abergel, J. R. Wallbank, X. Chen, M. Mucha-Kruczynski, V. I. Fal'ko, *New J. Phys.* **2013**, *15*, 123009.
[86] L. K. Li, Y. J. Yu, G. J. Ye, Q. Q. Ge, X. D. Ou, H. Wu, D. L. Feng, X. H. Chen, Y. B. Zhang, *Nat. Nanotechnol.* **2014**, *9*, 372.
[87] H. Liu, A. T. Neal, Z. Zhu, Z. Luo, X. F. Xu, D. Tomanek, P. D. Ye, *ACS Nano* **2014**, *8*, 4033.
[88] S. P. Koenig, R. A. Doganov, H. Schmidt, A. H. C. Neto, B. Ozyilmaz, *Appl. Phys. Lett.* **2014**, *104*, 103106.
[89] F. N. Xia, H. Wang, Y. C. Jia, *Nat. Commun.* **2014**, *5*, 4458.
[90] Y. Takao, A. Morita, *Physica B & C* **1981**, *105*, 93.
[91] H. Asahina, K. Shindo, A. Morita, *J. Phys. Soc. Jpn.* **1982**, *51*, 1193.
[92] J. S. Qiao, X. H. Kong, Z. X. Hu, F. Yang, W. Ji, *Nat. Commun.* **2014**, *5*, 4475.
[93] V. Tran, R. Soklaski, Y. F. Liang, L. Yang, *Phys. Rev. B* **2014**, *89*, 235319.
[94] T. Low, A. S. Rodin, A. Carvalho, Y. J. Jiang, H. Wang, F. N. Xia, A. H. C. Neto, *Phys. Rev. B* **2014**, *90*, 075429.
[95] S. Zhang, J. Yang, R. J. Xu, F. Wang, W. F. Li, M. Ghufran, Y. W. Zhang, Z. F. Yu, G. Zhang, Q. H. Qin, Y. R. Lu, *ACS Nano* **2014**, *8*, 9590.
[96] J. Yang, R. J. Xu, J. J. Pei, Y. W. Myint, F. Wang, Z. Wang, S. Zhang, Z. F. Yu, Y. R. Lu, *Light: Sci. Appl.* **2015**, *4*, e312.
[97] X. M. Wang, A. M. Jones, K. L. Seyler, V. Tran, Y. C. Jia, H. Zhao, H. Wang, L. Yang, X. D. Xu, F. N. Xia, *Nat. Nanotechnol.* **2015**, *10*, 517.

[98] L. Li, J. Kim, C. Jin, G. Ye, D. Y. Qiu, F. H. d. Jornada, Z. Shi, L. Chen, Z. Zhang, F. Yang, K. Watanabe, T. Taniguchi, W. Ren, S. G. Louie, X. Chen, Y. Zhang, F. Wang, *Nat. Nanotechnol.* **2016**, *12*, 21.
[99] A. Splendiani, L. Sun, Y. B. Zhang, T. S. Li, J. Kim, C. Y. Chim, G. Galli, F. Wang, *Nano Lett.* **2010**, *10*, 1271.
[100] K. F. Mak, C. Lee, J. Hone, J. Shan, T. F. Heinz, *Phys. Rev. Lett.* **2010**, *105*, 136805.
[101] C. H. Lee, G. H. Lee, A. M. van der Zande, W. C. Chen, Y. L. Li, M. Y. Han, X. Cui, G. Arefe, C. Nuckolls, T. F. Heinz, J. Guo, J. Hone, P. Kim, *Nat. Nanotechnol.* **2014**, *9*, 676.
[102] A. Pospischil, M. M. Furchi, T. Mueller, *Nat. Nanotechnol.* **2014**, *9*, 257.
[103] X. D. Duan, C. Wang, J. C. Shaw, R. Cheng, Y. Chen, H. L. Li, X. P. Wu, Y. Tang, Q. L. Zhang, A. L. Pan, J. H. Jiang, R. Q. Yu, Y. Huang, X. F. Duan, *Nat. Nanotechnol.* **2014**, *9*, 1024.
[104] B. W. H. Baugher, H. O. H. Churchill, Y. F. Yang, P. Jarillo-Herrero, *Nat. Nanotechnol.* **2014**, *9*, 262.
[105] K. F. Mak, K. L. He, J. Shan, T. F. Heinz, *Nat. Nanotechnol.* **2012**, *7*, 494.
[106] H. L. Zeng, J. F. Dai, W. Yao, D. Xiao, X. D. Cui, *Nat. Nanotechnol.* **2012**, *7*, 490.
[107] T. Cao, G. Wang, W. P. Han, H. Q. Ye, C. R. Zhu, J. R. Shi, Q. Niu, P. H. Tan, E. Wang, B. L. Liu, J. Feng, *Nat. Commun.* **2012**, *3*, 887.
[108] D. Xiao, G. B. Liu, W. X. Feng, X. D. Xu, W. Yao, *Phys. Rev. Lett.* **2012**, *108*, 196802.
[109] A. M. Jones, H. Y. Yu, N. J. Ghimire, S. F. Wu, G. Aivazian, J. S. Ross, B. Zhao, J. Q. Yan, D. G. Mandrus, D. Xiao, W. Yao, X. D. Xu, *Nat. Nanotechnol.* **2013**, *8*, 634.
[110] H. Y. Yu, Y. Wang, Q. J. Tong, X. D. Xu, W. Yao, *Phys. Rev. Lett.* **2015**, *115*, 187002.
[111] J. Lee, K. F. Mak, J. Shan, *Nat. Nanotechnol.* **2016**, *11*, 421.
[112] C. R. Dean, A. F. Young, I. Meric, C. Lee, L. Wang, S. Sorgenfrei, K. Watanabe, T. Taniguchi, P. Kim, K. L. Shepard, J. Hone, *Nat. Nanotechnol.* **2010**, *5*, 722.
[113] G. F. Schneider, V. E. Calado, H. Zandbergen, L. M. K. Vandersypen, C. Dekker, *Nano Lett.* **2010**, *10*, 1912.
[114] P. J. Zomer, S. P. Dash, N. Tombros, B. J. van Wees, *Appl. Phys. Lett.* **2011**, *99*, 232104.
[115] L. Wang, I. Meric, P. Y. Huang, Q. Gao, Y. Gao, H. Tran, T. Taniguchi, K. Watanabe, L. M. Campos, D. A. Muller, J. Guo, P. Kim, J. Hone, K. L. Shepard, C. R. Dean, *Science* **2013**, *342*, 614.
[116] Z. Liu, L. Song, S. Z. Zhao, J. Q. Huang, L. L. Ma, J. N. Zhang, J. Lou, P. M. Ajayan, *Nano Lett.* **2011**, *11*, 2032.
[117] Y. J. Gong, J. H. Lin, X. L. Wang, G. Shi, S. D. Lei, Z. Lin, X. L. Zou, G. L. Ye, R. Vajtai, B. I. Yakobson, H. Terrones, M. Terrones, B. K. Tay, J. Lou, S. T. Pantelides, Z. Liu, W. Zhou, P. M. Ajayan, *Nat. Mater.* **2014**, *13*, 1135.
[118] C. Zhang, S. Zhao, C. Jin, A. L. Koh, Y. Zhou, W. Xu, Q. Li, Q. Xiong, H. Peng, Z. Liu, *Nat. Commun.* **2015**, *6*, 6519.
[119] J. A. Miwa, M. Dendzik, S. S. Gronborg, M. Bianchi, J. V. Lauritsen, P. Hofmann, S. Ulstrup, *ACS Nano* **2015**, *9*, 6502.
[120] Q. Zhang, X. Xiao, R. Q. Zhao, D. H. Lv, G. C. Xu, Z. X. Lu, L. F. Sun, S. Z. Lin, X. Gao, J. Zhou, C. H. Jin, F. Ding, L. Y. Jiao, *Angew. Chem., Int. Ed.* **2015**, *54*, 8957.
[121] J. Feldmann, G. Peter, E. O. Gobel, P. Dawson, K. Moore, C. Foxon, R. J. Elliott, *Phys. Rev. Lett.* **1987**, *59*, 2337.
[122] S. Schmittrink, D. S. Chemla, D. A. B. Miller, *Adv. Phys.* **1989**, *38*, 89.
[123] K. F. Mak, J. Shan, *Nat. Photonics* **2016**, *10*, 216.
[124] C. Gong, H. J. Zhang, W. H. Wang, L. Colombo, R. M. Wallace, K. J. Cho, *Appl. Phys. Lett.* **2013**, *103*, 053513.
[125] H. P. Komsa, A. V. Krasheninnikov, *Phys. Rev. B* **2013**, *88*, 085318.
[126] J. Kang, S. Tongay, J. Zhou, J. B. Li, J. Q. Wu, *Appl. Phys. Lett.* **2013**, *102*, 012111.
[127] M. H. Chiu, C. D. Zhang, H. W. Shiu, C. P. Chuu, C. H. Chen, C. Y. S. Chang, C. H. Chen, M. Y. Chou, C. K. Shih, L. J. Li, *Nat. Commun.* **2015**, *6*, 7666.
[128] X. P. Hong, J. Kim, S. F. Shi, Y. Zhang, C. H. Jin, Y. H. Sun, S. Tongay, J. Q. Wu, Y. F. Zhang, F. Wang, *Nat. Nanotechnol.* **2014**, *9*, 682.
[129] F. Ceballos, M. Z. Bellus, H. Y. Chiu, H. Zhao, *ACS Nano* **2014**, *8*, 12717.
[130] H. Heo, J. H. Sung, S. Cha, B. G. Jang, J. Y. Kim, G. Jin, D. Lee, J. H. Ahn, M. J. Lee, J. H. Shim, H. Choi, M. H. Jo, *Nat. Commun.* **2015**, *6*, 7372.
[131] X. Y. Zhu, N. R. Monahan, Z. Z. Gong, H. M. Zhu, K. W. Williams, C. A. Nelson, *J. Am. Chem. Soc.* **2015**, *137*, 8313.
[132] A. F. Rigos, H. M. Hill, Y. L. Li, A. Chernikov, T. F. Heinz, *Nano Lett.* **2015**, *15*, 5033.
[133] P. Rivera, J. R. Schaibley, A. M. Jones, J. S. Ross, S. F. Wu, G. Aivazian, P. Klement, K. Seyler, G. Clark, N. J. Ghimire, J. Q. Yan, D. G. Mandrus, W. Yao, X. D. Xu, *Nat. Commun.* **2015**, *6*, 6242.
[134] H. L. Chen, X. W. Wen, J. Zhang, T. M. Wu, Y. J. Gong, X. Zhang, J. T. Yuan, C. Y. Yi, J. Lou, P. M. Ajayan, W. Zhuang, G. Y. Zhang, J. R. Zheng, *Nat. Commun.* **2016**, *7*, 12512.
[135] P. Rivera, K. L. Seyler, H. Y. Yu, J. R. Schaibley, J. Q. Yan, D. G. Mandrus, W. Yao, X. D. Xu, *Science* **2016**, *351*, 688.
[136] G. Eda, S. A. Maier, *ACS Nano* **2013**, *7*, 5660.
[137] K. S. Kim, Y. Zhao, H. Jang, S. Y. Lee, J. M. Kim, K. S. Kim, J. H. Ahn, P. Kim, J. Y. Choi, B. H. Hong, *Nature* **2009**, *457*, 706.
[138] F. Liu, S. Y. Song, D. F. Xue, H. J. Zhang, *Adv. Mater.* **2012**, *24*, 1089.
[139] G. Eda, G. Fanchini, M. Chhowalla, *Nat. Nanotechnol.* **2008**, *3*, 270.
[140] S. Bae, H. Kim, Y. Lee, X. F. Xu, J. S. Park, Y. Zheng, J. Balakrishnan, T. Lei, H. R. Kim, Y. I. Song, Y. J. Kim, K. S. Kim, B. Ozyilmaz, J. H. Ahn, B. H. Hong, S. Iijima, *Nat. Nanotechnol.* **2010**, *5*, 574.
[141] A. Ramasubramaniam, *Phys. Rev. B* **2012**, *86*, 115409.
[142] H. P. Komsa, A. V. Krasheninnikov, *Phys. Rev. B* **2012**, *86*, 241201(R).
[143] D. Y. Qiu, F. H. da Jornada, S. G. Louie, *Phys. Rev. Lett.* **2013**, *111*, 216805.
[144] A. Chernikov, T. C. Berkelbach, H. M. Hill, A. Rigosi, Y. L. Li, O. B. Aslan, D. R. Reichman, M. S. Hybertsen, T. F. Heinz, *Phys. Rev. Lett.* **2014**, *113*, 083603.
[145] Z. L. Ye, T. Cao, K. O'Brien, H. Y. Zhu, X. B. Yin, Y. Wang, S. G. Louie, X. Zhang, *Nature* **2014**, *513*, 214.
[146] J. He, N. Kumar, M. Z. Bellus, H. Y. Chiu, D. He, Y. Wang, H. Zhao, *Nat. Commun.* **2014**, *5*, 5622.
[147] M. Massicotte, P. Schmidt, F. Vialla, K. G. Schadler, A. Reserbat-Plantey, K. Watanabe, T. Taniguchi, K. J. Tielrooij, F. H. L. Koppens, *Nat. Nanotechnol.* **2016**, *11*, 42.
[148] T. Cao, Z. L. Li, D. Y. Qiu, S. G. Louie, *Nano Lett.* **2016**, *16*, 5542.
[149] M. Yankowitz, J. M. Xue, D. Cormode, J. D. Sanchez-Yamagishi, K. Watanabe, T. Taniguchi, P. Jarillo-Herrero, P. Jacquod, B. J. LeRoy, *Nat. Phys.* **2012**, *8*, 382.
[150] J. R. Wallbank, A. A. Patel, M. Mucha-Kruczynski, A. K. Geim, V. I. Falko, *Phys. Rev. B* **2013**, *87*, 245408.